Available online at www.sciencedirect.com
SCIENCE DIRECT
ELSEVIER
Icarus 177 (2005) 367–379
ICARUS
www.elsevier.com/locate/icarus

Mechanics of tidally driven fractures in Europa's ice shell

Sunwoong Lee [a], Robert T. Pappalardo [b], Nicholas C. Makris [a,*]

[a] *Department of Mechanical Engineering, Massachusetts Institute of Technology, Cambridge, MA 02139, USA*
[b] *Laboratory for Atmospheric and Space Physics and NASA Astrobiology Institute, University of Colorado, Boulder, CO 80309-0392, USA*

Received 19 July 2004; revised 16 June 2005
Available online 19 September 2005

Abstract

A fracture mechanics model is developed for the initiation and propagation of a crack through a porous ice layer of finite thickness under gravitational overburden. It is found that surface cracks generated in response to a tidally induced stress field may penetrate through the entire outer brittle layer if a subsurface ocean is present on Europa. Such penetration is found to be very unlikely in the absence of an ocean. A cycloidal crack would then form as a sequence of near instantaneous discrete failures, each extending roughly the brittle layer thickness in range, linked with a much lower apparent propagation speed set by the moving tidal stress field. The implications of this porous ice fracture model for ice-penetrating radar scattering loss and seismic activity are quantified.

Keywords: Europa; Ices; Porosity; Tides; Ocean; Fracture, cycloid; Radar

1. Introduction

Among Europa's surface features, cycloidal cracks are probably the most important for proving the existence of a subsurface liquid ocean. This is because (1) there is strong evidence that they are caused by tidally induced stress (Greenberg et al., 1998; Hoppa et al., 1999), and (2) this stress likely only approaches the ice failure strength if an ocean is present.

There are a number of outstanding issues, however, in quantitatively explaining cycloidal cracks. First, current estimates of the pure diurnal tidal stress necessary to cause cycloidal cracks even in the presence of an ocean range between 40 to 120 kPa based on kinematic fits to observed cycloid geometry (Hoppa et al., 1999, 2001; Crawford et al., 2005). This range is well below the typical stress known to cause tensile failure in natural terrestrial ice (Weeks and Assur, 1968; Vaudrey, 1977). Second, models of ridge formation suggest that cycloidal cracks penetrate through the entire brittle-ice layer (Hoppa et al., 1999; Pappalardo, 1999; Greeley et al., 2004a), but current models limit the depth of tidally induced surface cracks to be less than 100 m even in the presence of a europan ocean (Crawford and Stevenson, 1988; Hoppa et al., 1999; Lee et al., 2003; Greeley et al., 2004a). These penetration depths are more than an order of magnitude shallower than even the minimum current estimates of Europa's brittle layer thickness, which are in excess of 1 km (Ojakangas and Stevenson, 1989; Greenberg et al., 1998; Pappalardo, 1999; McKinnon, 1999; Deschamps and Sotin, 2001). Third, the 3-km/h crack propagation speed determined by Hoppa et al. (1999) is three orders of magnitude lower than the roughly 2-km/s speed at which cracks are known to propagate in ice (Freund, 1990).

The purpose of this paper is to quantitatively address these issues in a unified manner. To do this, a fracture mechanics model is developed for the initiation and propagation of a crack through an ice layer of finite thickness in the presence of gravitational overburden and porosity. It is found that surface cracks can penetrate through Europa's entire brittle layer, roughly a few kilometers, at the tidal stress thresholds found to be consistent with observed cycloid geometry in current kinematic models, if a liquid ocean is present under Europa's ice shell. Such penetration depths are found to be

* Corresponding author. Fax: +1 617 253 2350.
E-mail address: makris@mit.edu (N.C. Makris).

0019-1035/$ – see front matter
doi:10.1016/j.icarus.2005.07.003

extremely implausible in the absence of a liquid ocean because tidal stress levels are too low.

For crack initiation, it is shown that Europa's ice shell may be highly porous and salt-rich by use of terrestrial models and measurements (Weeks and Assur, 1968; Vaudrey, 1977) as well as Earth-based radar-wave backscattering data from Europa (Black et al., 2001a). This implies that the strength of Europa's outer ice shell may be sufficiently low to make the crack initiation strengths of 40–220 kPa arrived at by Hoppa et al. (1999, 2001) and Crawford et al. (2005) highly plausible, even though they are much lower than those typically measured for terrestrial ice.

For crack propagation, a model is developed for the stress intensity factor at a crack tip in an ice shell with finite thickness, gravitational overburden, and depth-dependent porosity. This leads to the conclusion that cycloids are generated as a sequence of discrete and near instantaneous fracture events, each of which penetrates through the entire brittle layer with horizontal length on the order of the brittle layer thickness. This mechanism yields an apparent propagation speed that is consistent with the 3-km/h crack propagation speed necessary to generate cycloids in current kinematic models (Hoppa et al., 1999, 2001; Gleeson et al., 2005). Total penetration would also provide paths for the emergence of water or ductile ice to form the observed ridges. Another implication of this model is that the level of seismic activity should be higher by orders of magnitude in the presence rather than absence of an ocean.

Both terrestrial sea ice measurements and radar backscattering data from Europa strongly suggest that Europa's ice is highly porous and the size of vacuous pores or salt pockets is on the order of a millimeter. Since the latter is at least three orders of magnitude smaller than the ice-penetrating radar wavelength, our calculations show that porosity-induced scattering should not be significant. This differs substantially from what has been predicted by Eluszkiewicz (2004), who arbitrarily assumed meter-scale spherical pores. Besides pores, fractures might constitute another class of void scatterers. Fractures, however, should only cause noticeable scattering if the surface normal of the fault exceeds the critical angle, typically 32° for electromagnetic waves incident from ice to vacuum and fracture opening widths are at least of radar-wavelength scale, which will likely be on the order of 1 m (Chyba et al., 1998; Blankenship et al., 1999). It is not yet clear if plausible mechanisms exist for maintaining such critically large opening widths.

2. Fracture initiation based on ice porosity

In current kinematic models for cycloidal cracks, the crack initiation threshold has been found to range from 40 to 120 kPa in the absence of stress accumulated by nonsynchronous rotation, if an ocean is present (Greenberg et al., 1998; Hoppa et al., 1999, 2001; Greenberg et al., 2003; Bart et al., 2003; Crawford et al., 2005). The typical strength of naturally occurring terrestrial ice, however, is roughly 500 kPa (Weeks and Assur, 1968; Vaudrey, 1977), which is roughly an order of magnitude larger than these crack initiation thresholds. Europa's ice shell would then require significantly lower strength for the current kinematic cycloidal crack models to be feasible.

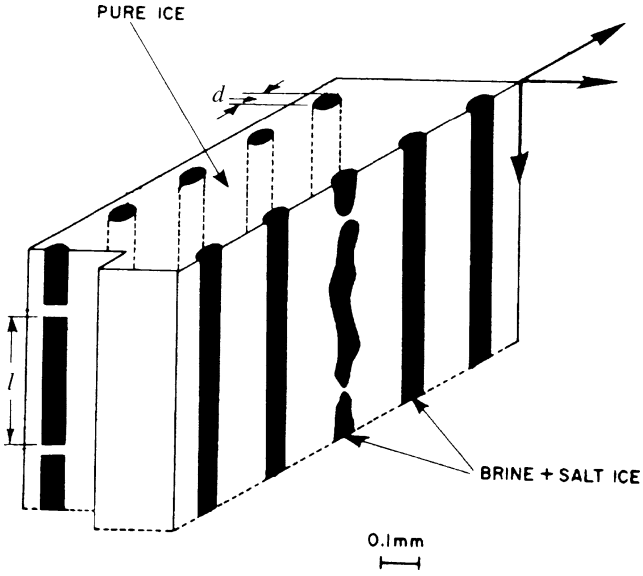

Fig. 1. The geometry of brine pockets in natural terrestrial sea ice (adapted from Weeks and Assur, 1968). Brine pockets generate cylindrical cavities with diameter d and length l.

This discrepancy can potentially be explained by examining the relationship between porosity and ice strength. The existence of pores and brine pockets in natural terrestrial sea ice has been known to decrease its strength significantly. Brine pockets generate cylindrical cavities in naturally grown ice, as shown in Fig. 1. Average values of the diameter d and the length l of the cylindrical pores in terrestrial ice are 0.07 and 0.23 mm, respectively (Anderson and Weeks, 1958). These cavities lead to a local magnification of stress near the cavities and a consequent decrease in the overall strength of the ice. Weeks and Assur (1968) have derived a semi-empirical relationship for the dependence of ice strength on porosity or brine content based on Arctic glacier and sea ice data assuming cylindrical cavities,

$$\sigma_f = \begin{cases} 6.86\times 10^5\left[1-\left(\dfrac{v_b}{0.202}\right)^{1/2}\right]\ \text{Pa} & \text{for } \sqrt{v_b} < 0.35, \\ 1.96\times 10^5\ \text{Pa} & \text{for } \sqrt{v_b} > 0.35, \end{cases} \quad (1)$$

where σ_f is the tensile strength of ice, and the dimensionless v_b is the fraction of volume occupied by pores, or the porosity. Vaudrey (1977) has derived a similar semi-empirical relationship independently from Antarctic glacier data, and has suggested that

$$\sigma_f = 9.59\times 10^5\left[1-\left(\frac{v_b}{0.249}\right)^{1/2}\right]\ \text{Pa}. \quad (2)$$

Table 1
Ice porosity of Galilean satellites estimated using 3.5- and 13-cm radar-wave observations (modified from Black et al., 2001a)

Wavelength	Europa	Ganymede	Callisto
3.5 cm	33%	2%	2%
13 cm	94%	5%	7%

These curves make it possible to quantitatively estimate the porosity necessary to obtain a given tensile strength. Given this, it may be determined if porosities corresponding to the crack initiation thresholds given in current kinematic models fall within a plausible range.

One may independently estimate the porosity of Europa's outer ice shell from Earth-based radar backscattering data. Black et al. (2001a) have investigated the effect of porosity on the measured radar reflectivity from Europa assuming spherical pores. The porosity of ice in their model can be obtained using

$$v_b = \int_{r_0}^{r_m} \frac{4\pi}{3} K r^{3-\beta}\, \mathrm{d}r, \tag{3}$$

where r is the radius of the pores, and r_0 and r_m are the minimum and the maximum radius of the pores. The constant K in Eq. (3) is given as

$$K = \frac{\tau_0}{l_i^0[1-e^{-\gamma}]}\left[\int_{r_0}^{r_m} r^{-\beta} C(r)\,\mathrm{d}r\right]^{-1}. \tag{4}$$

The physical explanations and the best-fit values of the parameters β, τ_0, γ and l_i^0 in Eqs. (3) and (4) are given in Table II and IV of Black et al. (2001a). The mean radius of the pores obtained from their best-fit values is 0.16 mm, which shows good agreement with the typical pore size in terrestrial ice previously discussed. Since most of the pores in their model are much smaller than the wavelengths of Earth-based radar, the detailed geometry of the pores is insignificant in the scattering model.

The resulting porosity estimates v_b for three icy satellites of Jupiter are shown in Table 1 for only the 3.5 and 13 cm radar observations since backscattering at 70 cm did not have sufficient signal-to-noise ratio (Black et al., 2001b) to be used for porosity estimation. It can be seen from Table 1 that Europa's porosity estimates are both variable and high compared to terrestrial levels, while those of Ganymede and Callisto are significantly lower and well in the terrestrial range.

The semi-empirical models of Weeks and Assur (1968) and Vaudrey (1977), shown in Fig. 2, begin with high tensile strength at the lowest porosities found in Antarctic and Arctic glaciers. Tensile strength monotonically decreases with increasing porosity until both models converge at the relatively high terrestrial porosities found in Arctic sea ice (Weeks and Anderson, 1958). Europa's porosity, as estimated from Earth-based radar backscatter data, exceeds the

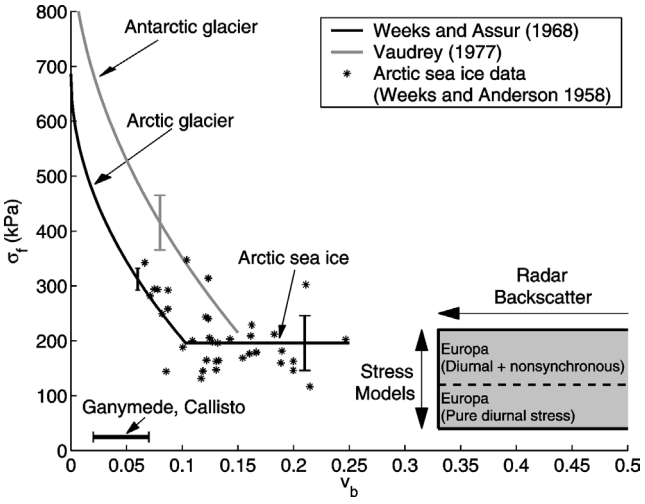

Fig. 2. Tensile strength σ_f of natural terrestrial ice as a function of porosity v_b. The shaded regime spans Europa's likely porosity range based on radar backscatter (Table 1) and the stress threshold range for cycloid formation from current kinematic models (Hoppa et al., 2001; Crawford et al., 2005). The likely porosity (Table 1) and the stress ranges on Ganymede and Callisto (Moore and Schubert, 2003) are also shown. The strength of clear lake ice typically varies from 600 to 750 kPa (Weeks and Assur, 1972).

maximum levels found in natural terrestrial ice. The porosities expected for Ganymede and Callisto from similar radar backscatter data put them in the porosity range of terrestrial glaciers.

The terrestrial ice strength curves of Fig. 2 show that the mean tensile strength of natural ice reaches a minimum value of 196 ± 50 kPa in the range $0.15 \leqslant v_b \leqslant 0.25$. No data exists beyond $v_b > 0.25$. A single extreme data point at 90 kPa for $v_b = 0.24$ (Fig. 9 of Schwarz and Weeks, 1977) indicates that occasionally lower strengths do occur. This may be used as a lower bound on tensile strengths for porosity $v_b \leqslant 0.25$. The maximum 220 kPa combined tidal and nonsynchronous stress threshold for cycloidal crack formation (Crawford et al., 2005) is consistent with crack initiation on Europa even if its porosity values fall within or exceed the upper range of those measured on Earth. Given this same range of porosities and the 90 kPa lower bound for tensile strength, it is possible that cracks occasionally initiate on Europa even under pure diurnal tidal forcing, with corresponding stress thresholds of 40–120 kPa (Hoppa et al., 1999; Crawford et al., 2005). It is reasonable to expect that as porosity increases above the values measured for terrestrial ice, the corresponding tensile strength will decrease. In this case, crack initiation on Europa becomes even more likely for the 40–220 kPa range of stress thresholds currently expected for cycloid formation. The upper limit allows for the addition of some nonsynchronous rotation stress (Greenberg et al., 1998; Crawford et al., 2005). In the absence of an ocean all tidally induced stress levels decrease by an order of magnitude, making it far less likely for cracks to initiate on Europa's surface.

The striking differences in surface geomorphology between Jupiter's three icy moons may be due to the differ-

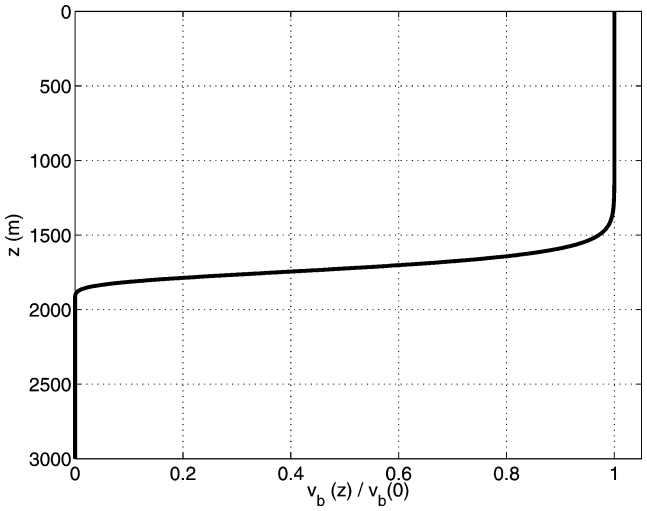

Fig. 3. Porosity profile versus depth z normalized by the surface porosity $v_b(0)$. The thickness of the brittle layer is assumed to be 3 km (adapted from Nimmo et al., 2003b).

ences in ice porosity. Tidal deformation and consequently tidal stress levels are roughly an order of magnitude lower on Ganymede and Callisto than on Europa (Moore and Schubert, 2003), as shown in Fig. 2. Given this and the fact that estimates from Earth-based radar backscattering data find the porosities of their outer shells to be much lower than Europa's, it seems implausible for tidally induced surface cracks to form regularly even if they have subsurface oceans. This can be seen in Fig. 2 where the failure stresses are at least an order of magnitude higher than the applied stresses on Ganymede and Callisto. This is consistent with the observation of no cycloidal surface fractures on Callisto (Greeley et al., 2000) or Ganymede (Prockter et al., 2000).

Pore closure due to gravitational overburden may lead to increasing ice strength with depth on Europa. The porosity of the ice shell versus depth can be estimated using the methods of Nimmo et al. (2003b), as shown in Fig. 3, where it is seen that high porosity may persist in the upper half of the brittle layer and approaches zero in the lower half of the layer. Together with Fig. 2, this indicates that tidally driven cracks on Europa are much more likely to initiate from the weaker outer surface of the ice shell rather than from the stronger base of the shell. Bottom-initiated cracks are also unlikely because of the high gravitational overburden pressure and ductility of warm ice at the base (Crawford and Stevenson, 1988). This is also consistent with terrestrial observation by Neave and Savage (1970) that, among more than 1000 ice cracking event samples in a roughly 300 m thick glacier, none originated at depths greater than 60 m.

One may then conclude that the combination of semi-empirical ice strength models and porosity estimates based on radar backscatter data from Europa suggests that cracks should at least occasionally initiate on Europa's surface under pure tidal stress for the thresholds given in current kinematic models for cycloids. Initiation would be more likely for the thresholds obtained under a combination of tidal and

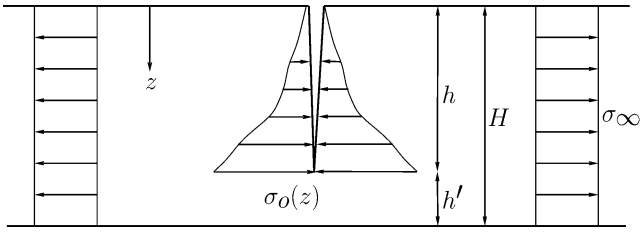

Fig. 4. Stresses applied to a surface crack with depth h in a brittle ice layer of thickness H, where σ_∞ is the local far-field tensile stress. The gravitational overburden stress $\sigma_0(z)$ on the crack walls is given in Eq. (A.1).

nonsynchronous stress (Crawford et al., 2005), or in concert with additional isotropic stress (Nimmo, 2004). Similar evidence suggests that it is unlikely for tidally induced surface cracks to form regularly on Ganymede and Callisto.

3. Fracture propagation

In the previous section, it was found that cracks can initiate on Europa's surface under currently hypothesized tensile stress levels, and with much higher probability if there is a liquid ocean present below its ice shell. Here we show that surface generated cracks on Europa may penetrate through the upper brittle layer of ice if the brittle layer is a few kilometers thick and if it is effectively decoupled from water or near-inviscid ductile ice below. We then argue that any given cycloidal arc on Europa's surface was likely formed as a sequence of concatenated cracks that penetrated through the entire brittle layer, so that the crack propagation speed determined by Hoppa et al. (1999, 2001) must then be an apparent speed.

3.1. Stress intensity factor as a function of crack depth in a finite ice shell

When a tensile stress field is applied to an elastic medium, cracks develop to release stress locally if the applied stress exceeds the medium's failure strength in tension. The direction of crack propagation is normal to the direction of applied tensile stress. On Europa, the elastic medium is also under the effect of gravitational overburden which exerts a linearly increasing compressive stress along the depth of the medium. This overburden stress suppresses crack propagation in the depth direction (Crawford and Stevenson, 1988; Hoppa et al., 1999; Greeley et al., 2004a).

The maximum penetration depth h of a surface-generated crack under the combination of a far-field tensile stress σ_∞ and a gravitational overburden compressive stress σ_o occurs roughly where these two opposing stresses cancel. A schematic diagram of crack geometry and stress distribution is shown in Fig. 4. The entire load from tensile stress σ_∞ is concentrated in the unfractured medium $h' = H - h$ below the crack since the fractured medium above cannot support tension. Here H is the thickness of either the entire ice shell which would be thin and brittle

(Ojakangas and Stevenson, 1989; Greenberg et al., 1998), or the upper brittle layer that is effectively decoupled from the ductile layer below (Pappalardo, 1999; McKinnon, 1999; Deschamps and Sotin, 2001). The tensile stress at the crack tip then increases nonlinearly as the crack grows in depth toward the lower boundary of the medium. The overburden compressive stress at the crack tip increases linearly as a function of h since the gravity force is a body force acting locally on the surface exposed by the fracture. A difference in depth dependence between tensile stress from far-field tidal forcing and compressive stress from overburden at the crack tip in the process of crack growth has been suggested in Leith and McKinnon (1996) and implied in Sandwell et al. (2004).

The stress intensity factor $K_{I,t}$ at the crack tip in an ice sheet due to far-field tensile stress σ_∞ is (Anderson, 1991; Tada et al., 2000)

$$K_{I,t}(\sigma_\infty, H, h) = \sigma_\infty \sqrt{\pi h} F\left(\frac{h}{H}\right), \tag{5}$$

where

$$F\left(\frac{h}{H}\right) = \sqrt{\frac{2H}{\pi h}\tan\frac{\pi h}{2H}} \times \frac{0.752 + 2.02(\frac{h}{H}) + 0.37(1-\sin\frac{\pi h}{2H})^3}{\cos\frac{\pi h}{2H}} \tag{6}$$

is a nonlinear function of the ratio of crack depth to the ice shell thickness h/H, with geometry shown in Fig. 4. The stress intensity factor $K_{I,t}$ approaches infinity as h/H approaches 1, as shown in Eqs. (5) and (6), due to the concentration of far-field tensile stress in the regime h' below the crack. As h/H approaches 0, Eq. (5) approaches the stress intensity factor obtained under the assumption that Europa's ice shell behaves as an infinite halfspace (Weertman, 1973; Smith, 1976; Crawford and Stevenson, 1988),

$$K_{I,t}(\sigma_\infty, h) \simeq 1.122\sigma_\infty\sqrt{\pi h}. \tag{7}$$

The stress intensify factor $K_{I,0}$ due to compressive stress from gravitational overburden is approximated as (Weertman, 1973; Hartranft and Sih, 1973; Smith, 1976)

$$K_{I,0}(h, h_p, v_b) \simeq -0.683\rho_i(1-v_b)gh\sqrt{\pi h} - u(h-h_p)\frac{2h\sqrt{h}}{\sqrt{\pi}}\rho_i v_b g \times \int_{\mathrm{asin}(h_p/h)}^{\pi/2}\left(\sin\theta - \frac{h_p}{h}\right) \times \left[1.3 - 0.3(\sin\theta)^{5/4}\right]\mathrm{d}\theta, \tag{8}$$

where ice density ρ_i is 920 kg/m^3, gravitational acceleration g is 1.32 m/s^2, and $u(h)$ is a unit step function. The compression from overburden acts locally on the crack with effectively no influence from the lower boundary. We assume that porosity persists up to the depth h_p from the surface,

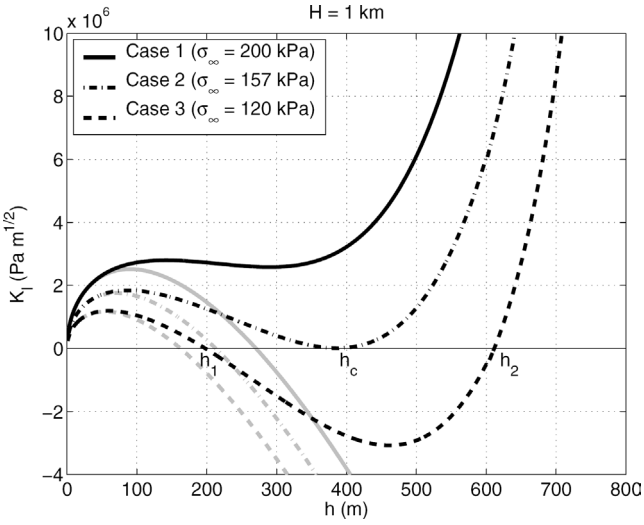

Fig. 5. The total stress intensity factor K_I for $H = 1$ km. Cases 1, 2, and 3 represent the no solution, 1 solution, and 2 solution cases in Eq. (9). The gray lines show the total stress intensity factors for corresponding cases when an infinite halfspace model is employed. The porosity of ice v_b is assumed to be zero.

where the depth of the porous layer h_p is taken to be roughly one half the thickness of the brittle layer based on the model of Nimmo et al. (2003b), as shown in Fig. 3.

3.2. Crack penetration depth

A surface-generated crack stops propagating at the depth where the stress intensity factor due to tension is balanced by the stress intensity factor due to overburden stress,

$$K_I(\sigma_\infty, H, h, h_p, v_b) = K_{I,t}(\sigma_\infty, H, h) + K_{I,0}(h, h_p, v_b) = 0. \tag{9}$$

If K_I is greater than zero, the crack propagates in depth to release the stress at the crack tip until K_I reaches zero. A negative stress intensity factor only has physical meaning in the sense that the crack cannot reach a depth where $K_I < 0$ since compression due to gravitational overburden overwhelms far-field tension at that depth. To find the depth of a tidally driven crack on Europa, Eq. (9) needs to be solved for h given H and σ_∞.

The stress intensity factor as a function of crack penetration depth h for an $H = 1$ km layer and a halfspace is illustrated in Fig. 5. If the fracture process is modeled under the assumption that the ice shell behaves as a halfspace, only a single solution is obtained. Crack penetration is then always limited to very shallow depths of roughly 200 m for pure diurnal tensile stress level of roughly 40–120 kPa (Hoppa et al., 1999; Crawford et al., 2005).

By including the finite thickness of the brittle ice layer in the fracture modeling, three possible forms of outcome must be considered, as illustrated in Fig. 5. In the first case, there is no mathematical solution to Eq. (9). This occurs when the far-field tensile stress σ_∞ is large enough that K_I in Eq. (9)

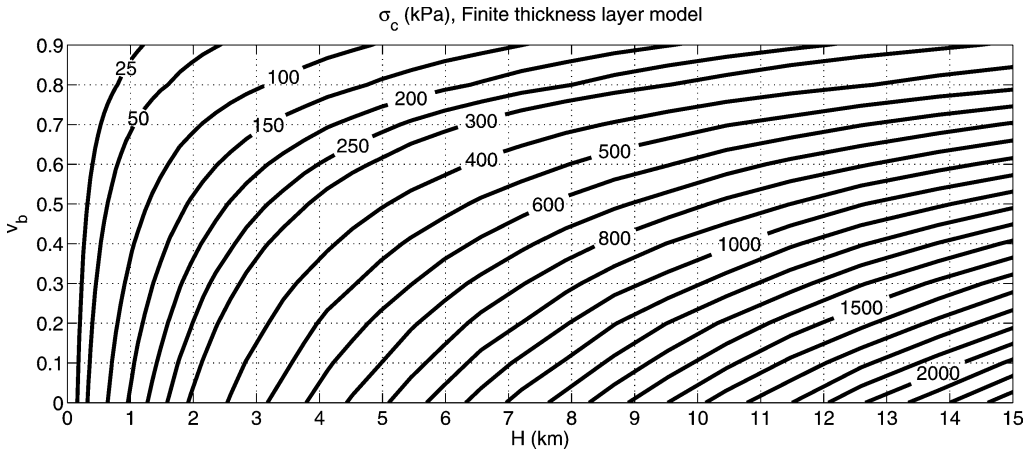

Fig. 6. The critical stress σ_c for total penetration through the brittle layer of thickness H and porosity v_b. The thickness of the porous layer h_p in Eq. (8) is assumed to be $H/2$ based on Nimmo et al. (2003b) and Fig. 3.

is always positive for $0 \leqslant h \leqslant H$. A surface-generated crack then penetrates rapidly through the entire brittle ice layer because the stress intensity factor at the crack tip always exceeds zero regardless of the crack depth h. In the second case, only one solution to Eq. (9) occurs. This occurs at critical depth $h = h_c$, but the solution is unstable. Given a minor overshoot of the crack tip beyond h_c (Freund, 1990), the stress intensity factor will become positive, where total penetration through the brittle ice layer will again occur. The far-field stress for the one solution case is the minimum required for total penetration through the entire layer H. This stress, defined as the critical stress σ_c, is a function of the layer thickness H. In the third case, the far-field stress is less than σ_c, and Eq. (9) has two solutions h_1 and h_2, where $0 < h_1 < h_2 < H$, as shown in Fig. 5. Given the exact deterministic Eqs. (5) and (8), the crack would only reach the shallower depth h_1 and stop. The shallower depth is similar to what one would obtain in the halfspace formulation. It is interesting that the depth scale of this shallower solution, given tidal forcing in the presence of an ocean, is similar to the 100-m-scale topographic variations on Europa's surface. It is also interesting that the expected pattern of stress relief due to these shallower surface cracks from tidal forcing is similar to the striated structure observed in many areas on Europa's surface.

The stress required for a crack to penetrate through the entire brittle layer H is shown in Fig. 6 as a function of ice porosity v_b and layer thickness H. We consider reasonable values for Europa's near-surface porosity to be within the 0.3–0.5 range. Current estimates of the far-field tidal stress necessary to match the geometry of observed cycloidal cracks range from 40 kPa for diurnal stress only (Hoppa et al., 1999) to 220 kPa for diurnal combined with nonsynchronous rotation stress (Crawford et al., 2005) if Europa possesses a liquid subsurface ocean. Within these bounds, surface generated cracks will penetrate through the entire brittle layer if its thickness does not exceed roughly 3 km. This limit on conductive layer thickness is consistent with those obtained based on thermal convection models (Deschamps and Sotin, 2001). Nonsynchronous stresses might be on the order of 500–1000 kPa, and could then lead to penetration through a significantly thicker brittle layer, on the order of 6–13 km. The resulting fractures, however, are not expected to be cycloidal because the total stress is dominated by the nonsynchronous stress components rather than the diurnal components (Hoppa, 1998; Crawford et al., 2005).

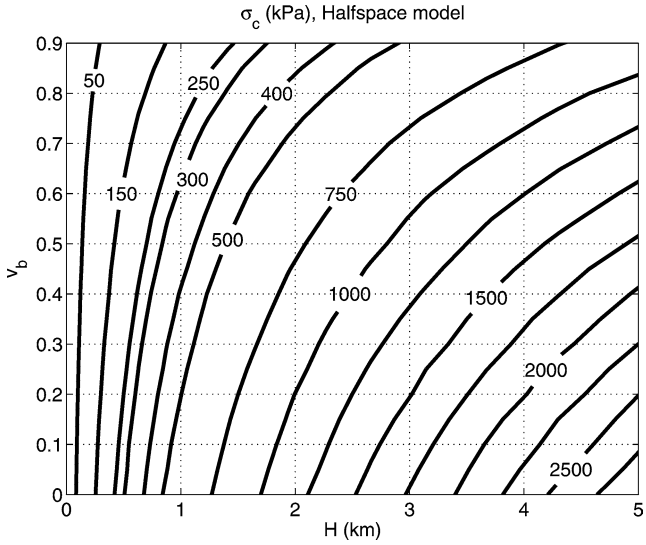

Fig. 7. The same as Fig. 6, but when Europa's brittle ice layer is assumed to be an infinite halfspace.

If the halfspace fracture model is employed, crack penetration depths are roughly a factor of 4–5 smaller within the same porosity and stress bounds, as shown in Fig. 7. These depths would not be consistent with cycloidal crack penetration through the entire brittle layer, based on most current estimates of its thickness.

From this fracture model and our current knowledge of the tidally induced stresses on Europa, we can draw the conclusion that the brittle layer should be less than a few kilometers in thickness, and should be mechanically decoupled

by water or weak convective ice below. We can also draw the conclusion that Europa should likely have an ocean of liquid water below its ice sheet. This can be inferred from Fig. 6, where the maximum outer layer thicknesses corresponding to full crack penetration would have to be less than an unreasonably small 100 m to fracture in response to the order of magnitude smaller tidal stress expected if Europa has no ocean (Moore and Schubert, 2000). Brittle layer thicknesses of less than 100 m are highly implausible because they do not even exceed the standard deviation of Europa's surface elevation (Prockter et al., 2002; Figueredo et al., 2002; Nimmo et al., 2003b).

3.3. Horizontal region of stress relief

The minimum length of a crack and region of stress relief in response to tension is on the order of the crack depth h when a surface crack develops in an elastic halfspace (Nur, 1982; Gudmundsson, 1987). If total penetration of a crack through the medium occurs, however, the region of stress relief is no longer limited by the crack depth, but is roughly proportional to the length of the crack (Timoshenko and Goodier, 1970). So as a crack extends in length, the region of stress relief, within which other long and deep cracks do not form, increases proportionally.

The minimum length of a crack that penetrates through the entire brittle layer would then be on the order of 1–3 km for pure diurnal tidal stress based on the findings of Section 3.2. Suppose, from a fully penetrating crack's initiation point up to some length at least one crack depth away in range, tidally induced stress exceeds the mean critical stress σ_c by an amount much larger than the critical stress standard deviation. The probability that the crack will exceed this length should then decrease rapidly because there is insufficient stress to maintain its propagation (Nur, 1982).

We believe that this is very likely the situation on Europa because (1) the spatial rate of change of tidal stress on Europa's surface is on the order of 1 kPa over a kilometer scale (Crawford et al., 2005), and (2) the corresponding stress change over the minimum length of a fully penetrating crack, roughly 1–3 km, is many times larger than the expected critical stress standard deviation, as shown in Appendix A.

3.4. Discrete fracture model for cycloidal crack propagation

Stress relief by fracture is nearly instantaneous because cracks in ice are expected to propagate at the 2-km/s Rayleigh wave speed, which is approximately 90% of the shear wave speed (Freund, 1990; Aki and Richards, 1980). Since this is three orders of magnitude larger than the roughly 3-km/h crack propagation speed (Hoppa et al., 1999; Gleeson et al., 2005), an additional physical mechanism must be considered to explain cycloid formation.

The stress field due to tidal forcing propagates with a speed that is orders of magnitude lower than the crack propagation speed since it is synchronized with the tidal bulge that slowly moves across Europa's surface. A crack that has penetrated through the entire brittle layer by the model of Sections 3.2 and 3.3 will not continue to propagate horizontally until the applied tidal stress field advected to the end tip of the crack reaches the critical stress.

Assuming the original crack extended in a direction normal to the direction of the maximum tensile principal stress at its space-time initiation point, the crack will extend in a new normal direction when it reinitiates at its former end tip because the direction of the maximum principal stress changes in time and space as a result of tidal forcing (Greenberg et al., 1998; Crawford et al., 2005). This reinitiated crack will again penetrate the entire brittle layer and propagate in range a distance roughly equal to the brittle layer thickness, wait for the threshold stress to move to the new end tip, and start the process all over. As the process continues, the series of discrete, temporally discontinuous, concatenated fractures through the entire brittle layer will form a cycloidal arc propagating at an *apparent* speed that is orders of magnitude slower than the Rayleigh speed. This *apparent* speed equals the rate of change of the tidally induced critical stress for total penetration of a crack through the brittle layer, varies with time and space, but should be within the range of 2–5 km/h found in the fits of Hoppa et al. (1999, 2001), Bart et al. (2003), Greenberg et al. (2003), and Gleeson et al. (2005) for pure diurnal stresses. A schematic diagram of cycloidal crack formation in this scenario is shown in Fig. 8. The use of these fitted speeds may not be practical for predicting new cycloids if the actual stress in the ice somehow begins to exceed the critical stress over an extended region. Fractures could then rapidly propagate near the Rayleigh speed across the extended region.

As noted in Section 3.3, stress will be relieved near the cycloidal arc over a proportionally larger region as it progresses. This will suppress development of other tidally induced cracks within a radius equaling roughly an arc length. This is consistent with observed cycloidal geometries (Fig. 3 of Hoppa et al., 1999), where it can be seen that the distance between the observable cycloids is roughly the length of a cycloidal arc.

As discussed in Hoppa et al. (1999), the cycloidal arc ends as Europa moves sufficiently far from pericenter. On the next day, a new tensile crack forms at this end, where stress concentration is largest, when the applied stress field again reaches the critical stress, σ_c. This initiates a new cycloidal arc linked to the end point of the previous one. Since the direction of the applied stress field changes drastically during the period of inactivity, the cycloid will exhibit a sharp cusp where the end of the old arc and the beginning of the new one meet.

Analogous observations have been made in terrestrial ice. Neave and Savage (1970) have shown that a sequence of more than 20 consecutive 10-m long tensile fractures formed

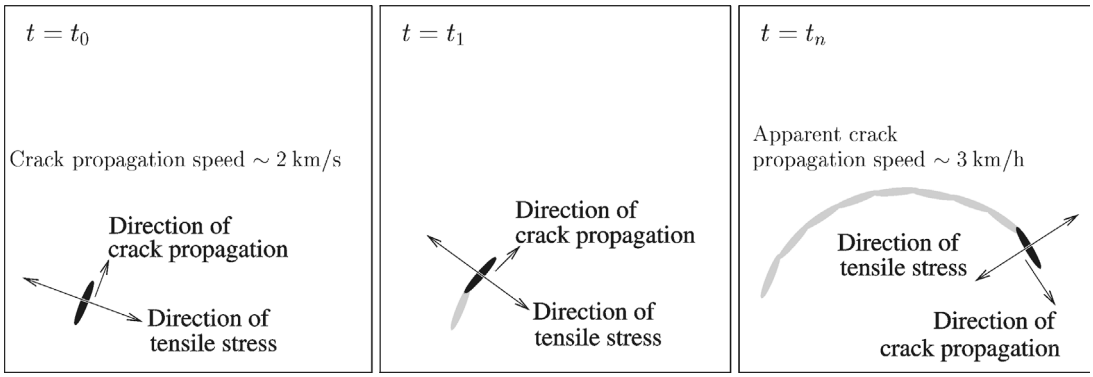

Fig. 8. Cycloidal crack formation under a temporally and spatially varying tensile stress field. A single crack penetrates through the entire brittle layer at time $t = t_0$ normal to the direction of maximum tensile stress over a fraction of a cycloidal arc. The crack forms "instantaneously" at roughly the Rayleigh speed. At a later time t_1, the fully penetrating crack reinitiates "instantaneously" in a slightly different direction when the threshold stress advects to the crack's former end tip. As the process continues, a series of discrete, temporally discontinuous, concatenated fractures through the entire brittle layer will form a cycloidal arc propagating at an *apparent* speed that is orders of magnitude slower than the Rayleigh speed, where t_n is the time of the nth discrete fracture. The cycloidal arc ceases to propagate when Europa moves so far from pericenter that the applied tensile stress tensor falls below the critical stress.

a several-hundred-meter long crevasse near the surface of an Arctic glacier. They have shown that the apparent propagation speed of the crevasse was 28 m/s, orders of magnitude smaller than the Rayleigh wave speed in ice. On Europa, a similar number of consecutive concatenated fractures form a cycloidal arc in our present model. Each discrete fracture in the cycloid penetrates through the entire brittle layer at roughly the Rayleigh speed. For the expected roughly 1–3 km brittle layer thickness, the penetration depths of these tensile fractures are equivalent to those that lead to the break up of Antarctic ice shelves, after accounting for the difference between the gravitational constants of Earth and Europa. Since the maximum instantaneous opening width of any initial tensile fracture should be on the order of a centimeter, while that of a full cycloid should be on the order of a meter (Timoshenko and Goodier, 1970), it is unlikely for extensive secondary fracturing and normal faulting to occur immediately.

An implication of this model is that the level of seismic activity should be higher by orders of magnitude in the presence of an ocean. High correlation is expected between the level of seismic activity and the tidal period in the presence but not in the absence of an ocean. This is because (1) tidal stresses are probably far too low to induce cracks in the absence of an ocean, and (2) surface cracks should form regularly during the tidal cycle if an ocean is present. The cracks associated with cycloids that fully penetrate the brittle layer should be at least 10^6 times more energetic than the shallow, roughly 100-m deep, surface cracks discussed in Section 3.2. The former should have center frequencies an order of magnitude lower than those of the latter. This will improve the signal-to-noise ratio for the type of seismic profiling discussed in Lee et al. (2003) if fully penetrating cracks are used as sources of opportunity. Since fully penetrating cracks are expected to occur on the order of once an hour for any given cycloid, the probability of unwanted overlap between different source signals and their multiple reflections is not high.

4. Ice-penetrating radar scattering loss

It has been proposed that Europa's potential subsurface ocean could be detected by ice-penetrating radar (Chyba et al., 1998; Moore, 2000). The main challenge to radar sounding on Europa lies in accrued absorption due to warm or dirty ice (Chyba et al., 1998; Moore, 2000), and scattering due to ice surface roughness and volume inhomogeneities (Greeley et al., 2004b; Blankenship et al., 1999). As shown in Section 2, Europa's ice shell may be highly porous, and as shown in Section 3, it may also be highly fractured. These inhomogeneities together with surface roughness will lead to scattering losses, the significance of which can be quantitatively assessed. Eluszkiewicz (2004) considered scattering losses from porosity on Europa. He arbitrarily assumed a pore radius of roughly 1 m, which is orders of magnitude larger than both that estimated from Earth-based radar measurements by Black et al. (2001a), and terrestrial ice rheology models as noted in Section 2. We show that this overestimation of pore size leads to a corresponding overestimation of transmission loss due to scattering by orders of magnitude.

The attenuation coefficient α of the mean electromagnetic field transmitted through a medium with inhomogeneities is (Rayleigh, 1899; van de Hulst, 1957)

$$\alpha = (10 \log e) N C \text{ dB/m}, \tag{10}$$

where N is the expected number density of scatterers per volume, and C is the expected scattering cross section of a given inhomogeneity. The scattering optical depth in Eq. (1) of Eluszkiewicz (2004) is related to α in Eq. (10) by

$$\tau_s^{\text{void}} = \alpha L/(10 \log e) = \frac{v_b}{4\pi r^3/3} Q(r) \pi r^2 L, \tag{11}$$

if the scatterers are arbitrarily assumed to be spherical as in Eluszkiewicz (2004), where L is the thickness of the scattering layer.

In general, the scattering cross section for spherical scatterers needs to be calculated using Mie theory, as in Fig. 9.

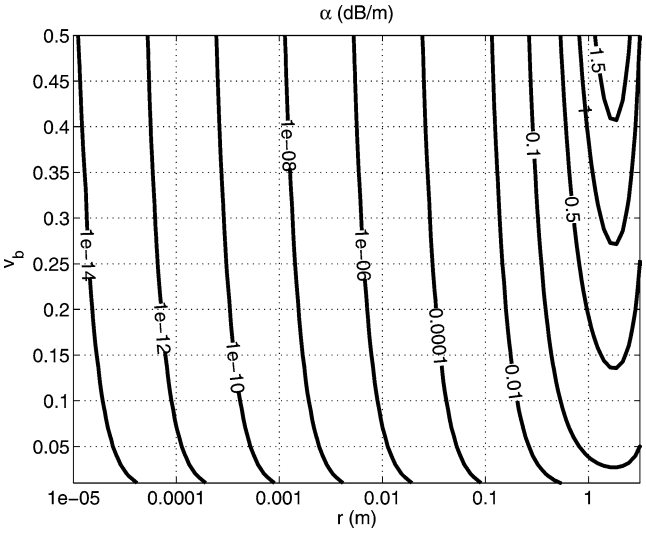

Fig. 9. Attenuation coefficient α from Eq. (10) as a function of porosity v_b and pore radius r, using exact Mie theory for scattering cross section C.

The expression for the scattering cross section, however, can be simplified using the Rayleigh scattering formula for $kr \ll 1$, or for $r \ll 0.5$ m at 50 MHz frequency,

$$C(r) \simeq \frac{8\pi}{3} k^4 r^6 \left| \frac{1-n_i^2}{1+2n_i^2} \right|^2, \tag{12}$$

where k is the wavenumber of the electromagnetic waves, and $n_i \simeq 1.8$ is the refractive index of ice (Gudmandsen, 1971). Then Eq. (10) can be simplified to (Rayleigh, 1899)

$$\alpha \simeq (20 \log e) v_b k^4 r^3 \left| \frac{1-n_i^2}{1+2n_i^2} \right|^2 \text{ dB/m}. \tag{13}$$

As can be seen from Eq. (13), attenuation by pores is linearly proportional to porosity v_b and the third power of pore radius r. Radar wave attenuation then increases dramatically with pore radius. The strong dependence of attenuation on scatterer size and distribution has long been demonstrated both theoretically and experimentally (Tyndall, 1893; Rayleigh, 1896). Since the pore size on Europa is expected to be on the millimeter scale, as discussed in Section 2, the attenuation coefficient α is approximately 10^{-6} dB/km for $v_b = 0.3$, as shown in Fig. 9. Assuming a 20 km thick ice shell, and conservatively assuming constant porosity from the surface to the bottom of Europa's ice shell, the two-way attenuation loss due to pores is then a negligible 10^{-4} dB. Arbitrarily assuming the meter-scale pores of Eluszkiewicz (2004) rather than the expected millimeter-scale pores leads to an extremely high attenuation loss of 100 dB/km, which is not observed in terrestrial ice-penetrating radar where total attenuation losses are only a few dB/km for cold ice (Gudmandsen, 1971). Even if pore closure by gravitational compaction is taken into account, Eluszkiewicz's meter-scale pore radius assumption still leads to an unprecedented 300 dB two-way transmission loss, for example, through a brittle layer of 3 km thickness. Since the loss for the expected millimeter scale pores is orders of magnitude less than the absorption loss due to warm ice or dirty ice (Chyba et al., 1998), ice-penetrating radar detectability will likely be far more challenged by absorption loss, rather than scattering loss due to pores.

For scattering from rough surfaces and fractured ice, a somewhat more accurate and in this case perhaps more insightful approach than that given in Eq. (10) would be to consider two-way transmission through a series of M layers. This would have a loss in the mean field due to scattering of (Rayleigh, 1899)

$$L_s = \sum_{j=0}^{1} \sum_{i=0}^{M} 20 \log\left(1 - m_i^j\right), \tag{14}$$

where the effective transmission coefficient $1 - m_i^j$ for the ith layer has negative reflection coefficient

$$m_i^j = \frac{N_i \, \mathrm{d}z_i C_i^j}{2}, \tag{15}$$

and N_i is the number of scatterers per unit volume, $\mathrm{d}z_i$ is the layer thickness, and C_i^j is the expected scattering cross section for inhomogeneities in the ith layer for a downward-directed wave ($j = 0$) and an upward-directed wave ($j = 1$).

Let us first consider a simple first-order estimate of the scattering loss from Europa's rough outer ice–vacuum boundary, the $i = 0$ layer. Assume that some fraction χ of the surface is inclined so that the angle between the local vertically directed incident plane wave and surface normal is greater than the critical angle, typically 32° for electromagnetic waves incident from ice to vacuum (see Fig. 10). Occlusion would not occur for a downward-directed plane wave from vacuum to ice making m_0^0 roughly zero, but it would occur for an upward-directed plane wave from ice to vacuum on the way back to the receiver making $m_0^1 = \chi$, as shown in Fig. 10. A total scattering loss in dB of $20 \log(1 - \chi)$ would be expected due to occlusion for this layer. Based on Europa's surface topography (Prockter et al., 2002; Figueredo et al., 2002; Nimmo et al., 2003a), a reasonable upper bound is roughly $\chi = 1/2$. This yields a total two-way loss of roughly 6 dB specifically for rough surface scattering, which is not a significant radar design impediment.

The expected scattering cross section C_i of fractures buried in the ice shell can be used to estimate radar attenuation due to scattering. While the opening width of a 100-km long cycloidal crack with total penetration through the brittle layer is expected to be on the order of a meter, based on linear elastic theory (Timoshenko and Goodier, 1970), these fractures will likely be filled by infiltration of liquid water or convective ice from below the layer and should not cause significant scattering. Shallow surface cracks that do not penetrate through the brittle layer are expected to be confined to the upper half of the brittle layer as shown in Section 3.4, and to have opening widths on the order of a millimeter to a centimeter (Nur, 1982;

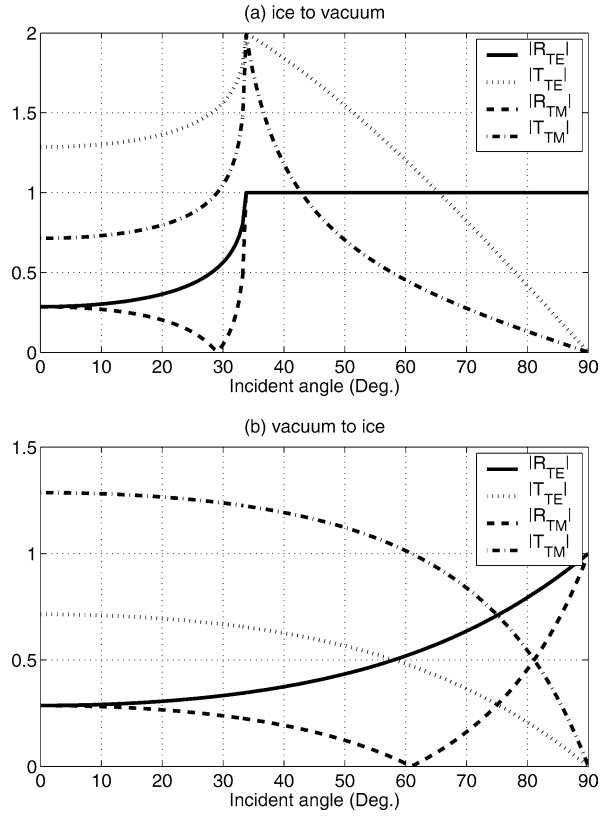

Fig. 10. Magnitude of reflection and transmission coefficients for a transverse electric ($R_{\mathrm{TE}}, T_{\mathrm{TE}}$) and a transverse magnetic ($R_{\mathrm{TM}}, T_{\mathrm{TM}}$) plane wave as a function of incident angle (Brekhovskikh, 1980; Kong, 2000). Propagation from (a) ice to vacuum interface, and (b) vacuum to ice interface. Total reflection occurs for incident angles greater than the 32° critical angle as can be seen in (a), where the magnitude of the reflection coefficients become unity.

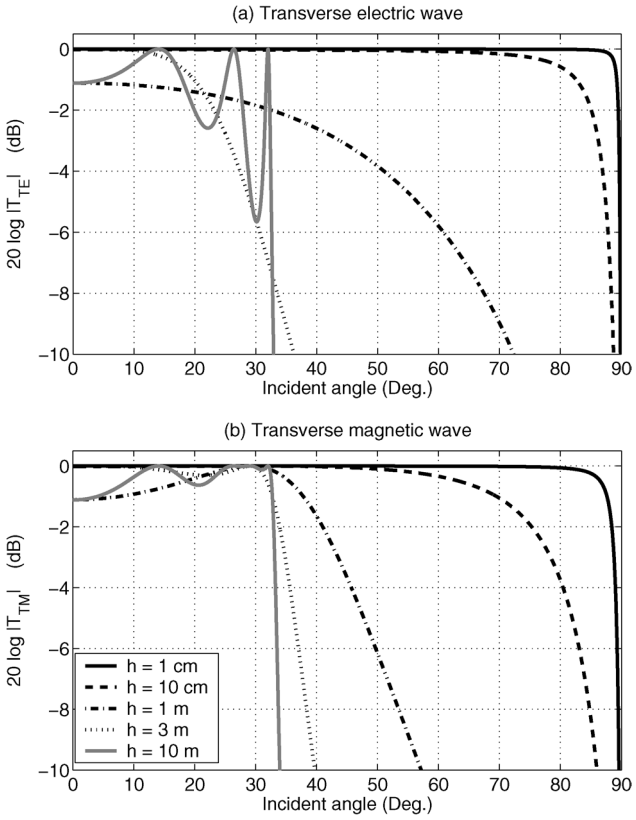

Fig. 11. Transmission coefficient of a transverse electric and a transverse magnetic plane wave through ice with a vacuum layer of thickness h. Even when the incident angle is below the critical angle, an evanescent component "tunnels" through the vacuum layer if its thickness is much smaller than the wavelength. The wavelength of the ice-penetrating radar waves is approximately 3 m at 50 MHz operating frequency. Transmission loss in dB per fracture is the negative of $20\log|T_{\mathrm{TE}}|$ or $20\log|T_{\mathrm{TM}}|$.

Lee et al., 2003). Since the tidally induced fractures considered so far are vertical, let us assume some mechanism exists by which the fracture plane is geologically rotated so that they will potentially affect ice-penetrating radar, such as the tectonic model of Manga and Sinton (2004).

Fractures should only cause noticeable transmission loss if (1) the angle between the surface normal and the direction of the incident waves exceeds the critical angle, and (2) the fracture opening widths are at least on the order of the wavelength to negate any significant tunneling of evanescent waves. This can be seen by inspection of Fig. 11, which shows transmission coefficients through ice with a planar vacuum layer of thickness h, or equivalently transmission loss in dB for an extended fracture, as a function of the incident angle and layer or fracture thickness. Current Earth-based radar measurements show far greater scattering cross sections for Europa for wavelengths at the centimeter rather than meter scale (Ostro et al., 1992; Black et al., 2001a, 2001b). This is consistent with our findings that tidally driven cracks that do not penetrate through the entire brittle layer have opening widths that probably do not exceed the centimeter scale and may be a significant source of radar scattering at these but not longer wavelengths, and that cracks that penetrate through the brittle layer should likely be filled in. Given this, there seems to be no compelling reason at the present time to expect the m_i^j for $i = 1, \ldots, M$ to be substantially different from zero for the meter-scale wavelengths of ice-penetrating radar missions under consideration for Europa (Chyba et al., 1998; Blankenship et al., 1999). This is consistent with terrestrial ice-penetrating radar scenarios in the Antarctic (Gudmandsen, 1971). It is not yet clear what mechanisms could be responsible for meter-scale or larger voids based on our current understanding of tidally driven fractures on Europa. Consequently, it is not yet clear whether any *scattering* mechanisms exist to significantly limit radar penetration of Europa's ice shell.

5. Conclusions

We find that surface cracks generated in response to a tidally induced stress field may penetrate through the entire brittle layer of Europa's ice shell, regardless of whether it lies directly above water or effectively inviscid warm ice, if a subsurface ocean exists. Such penetration is found to be unlikely in the absence of an ocean because tidal stresses

are then too low to induce deep cracks. A cycloidal crack would then form as a sequence of near instantaneous discrete failures, each extending in range on the order of the brittle layer thickness. Tidal forcing would link these fractures with an apparent speed corresponding to the low crack propagation speed derived by Hoppa et al. (1999). We have shown that ice-penetrating radar scattering losses due to porosity are likely to be negligible since pores are expected to be extremely small compared to the wavelength. While fractures with opening widths of at least the wavelength scale may affect ice-penetrating radar, it seems unlikely that such openings could remain sufficiently void and occur with sufficient spatial frequency to significantly limit radar penetration. We have also shown that the level of seismic activity should be higher by orders of magnitude if an ocean is present on Europa.

Acknowledgment

The first sentence of introduction paraphrases comments made by Torrence Johnson at and before the Workshop on Europa's Icy Shell 2004 in reference to the work of Hoppa, Tufts, Greenberg, and Geissler (1999).

Appendix A. Standard deviation and bias of critical stress in an ice shell with random depth-dependent porosity

We show that the standard deviation and bias of critical stress σ_c due to fluctuation of ice porosity v_b as a function of depth is appreciably smaller than the 1 kPa spatial change of tidal stress expected on Europa's surface over 1 km, roughly the minimum length of a fully penetrating crack. The compressive stress $\sigma_0(z)$ due to gravitational overburden is given by

$$\sigma_0(z) = \int_0^z \rho(z_0) g \, \mathrm{d}z_0, \tag{A.1}$$

where $\rho(z)$ is the density of a medium. The stress intensity factor $K_{I,0}$ due to σ_0 is (Tada et al., 2000),

$$K_{I,0}(h) = -\int_0^h f(z)\sigma_0(z) \, \mathrm{d}z, \tag{A.2}$$

where

$$f(z) = \frac{2}{\sqrt{\pi h}} \frac{1.3 - 0.3(z/h)^{5/4}}{\sqrt{1-(z/h)^2}}. \tag{A.3}$$

Then the variance of the stress intensity factor in Eq. (A.2) is

$$\mathrm{Var}\big(K_{I,0}(h)\big) = \int_0^h \int_0^h f(z) f(z') \, \mathrm{Cov}\big(\sigma_0(z), \sigma_0(z')\big) \, \mathrm{d}z \, \mathrm{d}z', \tag{A.4}$$

where

$$\mathrm{Cov}\big(\sigma_0(z), \sigma_0(z')\big) = g^2 \int_0^z \int_0^{z'} \mathrm{Cov}\big(\rho(z_0), \rho(z_0')\big) \, \mathrm{d}z_0 \, \mathrm{d}z_0'. \tag{A.5}$$

We take the covariance of density to be

$$\begin{aligned}\mathrm{Cov}\big(\rho(z_0), \rho(z_0')\big) &= z_c \delta(z_0 - z_0') \, \mathrm{Var}\big(\rho(z_0)\big) \\ &= z_c \delta(z_0 - z_0') \rho_i^2 \, \mathrm{Var}\big(v_b(z_0)\big),\end{aligned} \tag{A.6}$$

where z_c is the correlation length of density versus depth. Fluctuating density contributions to the variance of the stress intensity factor then accumulate incoherently with depth. We take the correlation length z_c to be roughly the pore size, which is expected to be less than 1 mm based on terrestrial values and estimates of Europa's pore size given in Section 2.

The variance of the stress intensity factor in Eq. (A.2) is then

$$\mathrm{Var}\big(K_{I,0}(h)\big) = g^2 z_c \rho_i^2 \, \mathrm{Var}(v_b) \int_0^h f(z) \left[\int_0^z z' f(z') \, \mathrm{d}z' \right] \mathrm{d}z \tag{A.7}$$

using Eqs. (A.5) and (A.6). Here we have neglected pore closure due to gravitational compaction, and assumed that porosity obeys a stationary random process across depth so that $\mathrm{Var}(v_b(z_0)) \equiv \mathrm{Var}(v_b)$. When the mean to standard deviation ratio of critical stress is large, its asymptotic variance becomes (Naftali and Makris, 2001)

$$\mathrm{Var}(\sigma_c) = \left(\frac{\partial \sigma_c}{\partial K_{I,0}(h_c)} \right)^2 \mathrm{Var}\big(K_{I,0}(h_c)\big), \tag{A.8}$$

and the bias of the critical stress

$$\mathrm{bias}(\sigma_c) = \big\langle \sigma_c(v_b) \big\rangle - \sigma_c(v_b) \tag{A.9}$$

is asymptotically

$$\mathrm{bias}(\sigma_c) = -\frac{1}{2} \frac{\partial^2 \langle v_b \rangle}{\partial \sigma_c^2} \big(\mathrm{Var}(v_b)\big)^{-1} \frac{\partial \langle v_b \rangle}{\partial \sigma_c} \big(\mathrm{Var}(\sigma_c)\big)^2. \tag{A.10}$$

Our numerical simulations show that the standard deviation of the critical stress σ_c calculated using Eq. (A.8) is roughly 0.1 kPa and the bias is effectively zero for a brittle layer of ice with a few kilometer thickness. Here it is conservatively assumed that $z_c = 1$ mm and v_b follows a uniform distribution from 0 to 1.

References

Aki, K., Richards, P.G., 1980. Quantitative Seismology. Freeman, San Francisco.

Anderson, D.L., Weeks, W.F., 1958. A theoretical analysis of sea-ice strength. Trans. Am. Geophys. Union 39, 632–640.

Anderson, T.L., 1991. Fracture Mechanics: Fundamentals and Applications. CRC Press, Boca Raton, FL.

Bart, G.D., Greenberg, R., Hoppa, G.V., 2003. Cycloids and wedges: Global patterns from tidal stresses on Europa. Lunar Planet. Sci. XXXIV. Abstract 1396.

Black, G.J., Campbell, D.B., Nicholson, P.D., 2001a. Icy Galilean satellites: Modeling radar reflectivities as a coherent backscatter effect. Icarus 151, 167–180.

Black, G.J., Campbell, D.B., Ostro, S.J., 2001b. Icy Galilean satellites: 70 cm radar results from Arecibo. Icarus 151, 160–166.

Blankenship, D.D., Edwards, B.C., Kim, Y., Geissler, P.E., Gurnett, D., Johnson, W.T.K., Kofman, W., Moore, J.C., Morse, D.L., Pappalardo, R.T., Picardi, G., Raney, R.K., Rodriguesz, E.R., Shao, X.M., Weerman, J., Zebker, H.A., van Zyl, J., 1999. Feasibility study and design concept for an orbiting ice-penetrating radar sounder to characterize in three-dimensions the europan ice mantle down to (and including) any ice/ocean interface, Technical report 184. University of Texas, Austin.

Brekhovskikh, L.M., 1980. Waves in Layered Media, second ed. Academic Press, New York.

Chyba, C.F., Ostro, S.J., Edwards, B.C., 1998. Radar detectability of a subsurface ocean on Europa. Icarus 134, 292–302.

Crawford, G.D., Stevenson, D.J., 1988. Gas driven water volcanism and the resurfacing of Europa. Icarus 73, 66–79.

Crawford, Z., Pappalardo, R.T., Barr, A., Gleeson, D., Mullen, M., Nimmo, F., Stempel, M.M., Wahr, J., 2005. Wavy lineaments on Europa: Fracture propagation into combined nonsynchronous and diurnal stress fields. Lunar Planet. Sci. XXXVI. Abstract 2042.

Deschamps, F., Sotin, C., 2001. Thermal convection in the outer shell of large icy satellites. J. Geophys. Res. 106, 5107–5121.

Eluszkiewicz, J., 2004. Dim prospects for radar detection of Europa's ocean. Icarus 170, 234–236.

Figueredo, P.H., Chuang, F.C., Rathbun, J., Kirk, R.L., Greeley, R., 2002. Geology and origin of Europa's mitten feature (Murias Chaos). J. Geophys. Res. 107, 10.1029/2001JE001591.

Freund, L.B., 1990. Dynamic Fracture Mechanics. Cambridge Univ. Press, New York.

Gleeson, D., Crawford, Z., Barr, A.C., Mullen, M., Pappalardo, R.T., Prockter, L.M., Stempel, M.M., Wahr, J., 2005. Wavy and cycloidal lineament formation on Europa from combined diurnal and nonsynchronous stresses. Lunar Planet. Sci. XXXVI. Abstract 2364.

Greeley, R., Klemaszewski, J.E., Wagner, R., the Galileo Imaging Team, 2000. Galileo views of the geology of Callisto. Planet. Space Sci. 48, 829–853.

Greeley, R., Chyba, C., Head III, J.W., McCord, T., McKinnon, W.B., Pappalardo, R.T., Figueredo, P., 2004a. Geology of Europa. In: Bagenal, F., Dowling, T.E., McKinnon, W.B. (Eds.), Jupiter: The Planet, Satellites, and Magnetosphere. Cambridge Univ. Press, New York, pp. 329–362.

Greeley, R., Johnson, T., the JIMO Science Definition Team, 2004b. Report of the NASA Science Definition Team for the Jupiter Icy Moons Orbiter, Technical report. NASA.

Greenberg, R., Geissler, P., Hoppa, G., Tufts, B.R., Durda, D.D., Pappalardo, R.T., Head, J.W., Greeley, R., Sullivan, R., Carr, M.H., 1998. Tectonic processes on Europa: Tidal stresses, mechanical response, and visible features. Icarus 135, 64–78.

Greenberg, R., Hoppa, G.V., Bart, G., Hurford, T., 2003. Tidal stress patterns on Europa. Celest. Mech. Dyn. Astron. 87, 171–188.

Gudmandsen, P., 1971. Electromagnetic probing of ice. In: Wait, J.R. (Ed.), Electromagnetic Probing in Geophysics. The Golem Press, Boulder, pp. 321–348.

Gudmundsson, A., 1987. Tectonics of the Thingvellir fissure swarm, SW Iceland. J. Struct. Geol. 9, 61–69.

Hartranft, R.J., Sih, G.C., 1973. Alternating method applied to edge and surface crack problems. In: Sih, G.C. (Ed.), Methods of Analysis and Solutions of Crack Problems. Noordhoff, Leyden, pp. 179–238, ch. 4.

Hoppa, G.V., 1998. Europa: Effects of rotation and tides on tectonic processes. Ph.D. thesis, Univ. of Arizona, Tucson.

Hoppa, G.V., Tufts, B.R., Greenberg, R., Geissler, P.E., 1999. Formation of cycloidal features on Europa. Science 285, 1899–1902.

Hoppa, G.V., Tufts, B.R., Greenberg, R., Hurford, T.A., O'Brien, D.P., Geissler, P.E., 2001. Europa's rate of rotation derived from the tectonic sequence in the Astypalaea region. Icarus 153, 208–213.

Kong, J.A., 2000. Electromagnetic Wave Theory. EMW Publishing, Cambridge.

Lee, S., Zanolin, M., Thode, A.M., Pappalardo, R.T., Makris, N.C., 2003. Probing Europa's interior with natural sound sources. Icarus 165, 144–167.

Leith, A.C., McKinnon, W.B., 1996. Is there evidence for polar wander on Europa? Icarus 120, 387–398.

Manga, M., Sinton, A., 2004. Formation of bands and ridges on Europa by cyclic deformation: Insights from analogue wax experiments. J. Geophys. Res. 109, E09001, 10.1029/2004JE002249.

McKinnon, W.B., 1999. Convective instability in Europa's floating ice shell. Geophys. Res. Lett. 26, 951–954.

Moore, J.C., 2000. Models of radar absorption in europan ice. Icarus 147, 292–300.

Moore, W.B., Schubert, G., 2000. The tidal response of Europa. Icarus 147, 317–319.

Moore, W.B., Schubert, G., 2003. The tidal response of Ganymede and Callisto with and without liquid water oceans. Icarus 166, 223–226.

Naftali, E., Makris, N.C., 2001. Necessary conditions for a maximum likelihood estimate to become asymptotically unbiased and attain the Cramer–Rao lower bound. Part I. General approach with an application to time-delay and Doppler shift estimation. J. Acoust. Soc. Am. 110, 1917–1930.

Neave, K.G., Savage, J.C., 1970. Icequakes on the Athabasca glacier. J. Geophys. Res. 75, 1351–1362.

Nimmo, F., 2004. Stresses generated in cooling viscoelastic ice shell: Application to Europa. J. Geophys. Res. 109, E12001, 10.1029/2004JE002347.

Nimmo, F., Giese, B., Pappalardo, R.T., 2003a. Estimates of Europa's ice shell thickness from elastically supported topography. Geophys. Res. Lett. 30, 10.1029/2002GL016660.

Nimmo, F., Pappalardo, R.T., Giese, B., 2003b. On the origins of band topography, Europa. Icarus 166, 21–32.

Nur, A., 1982. The origin of tensile fracture lineaments. J. Struct. Geol. 4, 31–40.

Ojakangas, G.W., Stevenson, D.J., 1989. Thermal state of an ice shell on Europa. Icarus 81, 220–241.

Ostro, S.J., Campbell, D.B., Simpson, R.A., Hudson, R.S., Chandler, J.F., Rosema, K.D., Shapiro, I.I., Standish, E.M., Winkler, R., Yeomans, D.K., Goldstein, R.M., 1992. Europa, Ganymede, and Callisto: New radar results from Arecibo and Goldstone. J. Geophys. Res. 97, 18227–18244.

Pappalardo, R.T., 31 colleagues, 1999. Does Europa have a subsurface ocean? Evaluation of the geological evidence. J. Geophys. Res. 104, 24015–24055.

Prockter, L.M., Figueredo, P.H., Pappalardo, R.T., Head III, J.W., Collins, G.C., 2000. Geology and mapping of dark terrain on Ganymede and implications for grooved terrain formation. J. Geophys. Res. 105, 22519–22540.

Prockter, L.M., Head III, J.W., Pappalardo, R.T., Sullivan, R.J., Clifton, A.E., Giese, B., Wagner, R., Neukum, G., 2002. Morphology of Europan bands at high resolution: A mid-ocean ridge-type rift mechanism. J. Geophys. Res. 107, 10.1029/2000JE001458.

Rayleigh, J.W.S., 1896. The Theory of Sound, second ed., vol. 2. Macmillan, London.

Rayleigh, J.W.S., 1899. On the transmission of light through an atmosphere containing small particles in suspension, and on the origin of the blue of the sky. Philos. Mag. 47, 375–384.

Sandwell, D., Rosen, P., Moore, W., Gurrola, E., 2004. Radar interferometry for measuring tidal strains across cracks on Europa. J. Geophys. Res. 109, E11003, 10.1029/2004JE002276.

Schwarz, J., Weeks, W.F., 1977. Engineering properties of sea ice. J. Glaciol. 19, 499–531.

Smith, R.A., 1976. The application of fracture mechanics to the problems of crevasse penetration. J. Glaciol. 17, 223–228.

Tada, H., Paris, P.C., Irwin, G.R., 2000. The Stress Analysis of Cracks Handbook, third ed. ASME Press, New York.

Timoshenko, S.P., Goodier, J.N., 1970. Theory of Elasticity, third ed. McGraw–Hill, New York.

Tyndall, J., 1893. Sound, fifth ed. Longmans, Green, London.

van de Hulst, H.C., 1957. Light Scattering by Small Particles. Wiley, New York.

Vaudrey, K.D., 1977. Ice engineering—Study of related properties of floating sea-ice sheets and summary of elastic and viscoelastic analyses. Technical Report TR-860. Civil Engineering Laboratory, Alexandria.

Weeks, W.F., Anderson, D.L., 1958. An experimental study of strength of young sea ice. Trans. Am. Geophys. Union 39, 641–647.

Weeks, W.F., Assur, A., 1968. The mechanical properties of sea ice. In: Ice Pressures against Structures, Assoc. Committee on Geotech. Res. of the Natl. Res. Council of Canada, Ottawa. Proceedings of a Conference held at Laval University, Quebec, 10–11 November 1966. Tech. Memo. No. 92, pp. 25–78.

Weeks, W.F., Assur, A., 1972. Fracture of lake and sea ice. In: Liebowitz, H. (Ed.), Fracture, An Advanced Treatise, vol. 7. Academic Press, New York, pp. 879–978.

Weertman, J., 1973. Can a water-filled crevasse reach the bottom surface of a glacier? In: Symposium on the Hydrology of Glaciers, Cambridge, 7–13 Sept. 1969. International Association of Hydrologic Sciences, Cambridge, pp. 139–145.